The Chemical Engineering Journal, 17 (1979) 81 - 89

Hydrodynamic Behaviour of a Gas–Solid Counter-current Packed Column at Trickle Flow

A. W. M. ROES and W. P. M. VAN SWAAIJ
Twente University of Technology, Enschede (The Netherlands)
(Received 12 December 1977)

Abstract

Trickle flow of a more or less fluidized catalyst through a packed column is a promising new gas–solid counter-current operation. The hydrodynamic behaviour of such a column, filled with dumped PALL rings, has been investigated, while some results have been obtained with RASCHIG rings and cylindrical screens as packing. The solid used was a microspherical catalyst carrier. Pressure drop, hold-up, loading and flooding were evaluated and compared with literature data for gas–liquid systems. The behaviour is analogous although the absolute magnitude is different.

Pressure drop is low, up to 50% of the solid being carried by the packing. A correlation for the pressure drop, which is mainly caused by suspended particles, has been derived. At low gas velocities particle velocity is constant, whilst near flooding the slip velocity between gas and solid reaches a constant value. Using empirical values for particle velocity and slip velocity, hold-up, loading and flooding can be predicted. Scaling-up problems still need to be investigated. Results on mass transfer, axial dispersion of both phases and solid spread factors will be published later.

1. INTRODUCTION

In gas–solid counter-current processes, like purification, separation, component recovery, drying or chemical reaction, five types of reactors can be distinguished, namely spray columns, moving beds, multi-stage fluid beds, zig-zag contactors and packed columns (Fig. 1). For ideal behaviour counter-current adsorbers should have plug flow in both phases and a high mass transfer rate between them. Spray columns [1], which offer the advantage of simplicity, show an important top-to-bottom mixing of gas and solid. Mixing in both phases can be reduced by using a dense solid system (moving bed) or by using internals (c - e). Moving beds [1, 2] exhibit a high gas-to-particle mass transfer rate, although the pressure drop is high, especially with small particles and at high gas flow rates. It is also difficult to maintain a constant solid flow, a radial velocity profile of the particles exists and radial heat conductivity is low. A high flow rate of solid matter, especially with small particles, can be obtained in a zig-zag contactor [3], which is used in the petrochemical industry for stripping purposes of large solid flows, *e.g.* in catalytic cracking units. Multi-stage fluid beds [4, 5] are frequently used in counter-current adsorption processes and as chemical reactors/heat exchangers. Axial mixing of gas and solid is low, temperature control is easy but pressure drop can be considerable. It is difficult to achieve an even gas distribution for each plate, resulting in a not very flexible

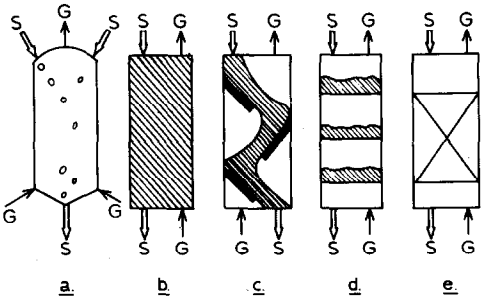

Fig. 1. Gas–solid counter-current contactors: ⇒, direction of solid; →, direction of gas. a, spray column; b, moving bed; c, zig-zag contactor; d, multi-stage fluid bed; e, packed column.

operation. Recently, however, methods have been developed to change the free area per plate during operation [6], so that flexibility can be improved.

The difficulties related to a multi-stage fluid bed may be overcome in a packed column. As in gas–liquid operation, packing is inserted in the column to reduce axial mixing of gas and particles, to redistribute and carry the solid and to facilitate mass transfer. Very little is known about gas–solid counter-current packed columns. Preliminary studies on the hydrodynamic behaviour of such an apparatus have been carried out by Claus *et al.* [7, 8]. They used a column filled with dumped cylindrical screens, while under counter-current operation sand and vegetable abrasive were used as solid material. They found flow regions comparable with gas–liquid systems: a continuous dense phase region, where gas bubbles rise through a dense bed of particles, and a trickle flow region, where trickles of solids fall down over the packing.

Trickle flow seems to be attractive owing to the low pressure drop and axial mixing, high mass transfer and easy construction of the equipment. Applications may be in the field of chemical reactors, *e.g.* for flue gas cleaning, counter-current adsorption processes, continuous gas chromatography, etc. We investigated trickle flow of a highly porous catalyst carrier in packed columns of PALL rings; some results have also been obtained for RASCHIG rings and cylindrical screens. The present investigation deals with results on hydrodynamic behaviour. Results on axial mixing mass transfer and solids spreading over the packing will be reported later [9].

2. EXPERIMENTAL SYSTEM

The experimental set-up is shown in Fig. 2. A Pyrex column, 1.00 m in length with an internal diameter of 0.0755 m and filled with dumped rings, is mounted on a fluid bed via a perspex section. The latter contains two valves V_1 and V_3 made of brass with an O ring at the edge. V_2 is a similar valve containing a porous glass plate distributor.

Air enters the column via a porous plate distributor. It passes through the packing and

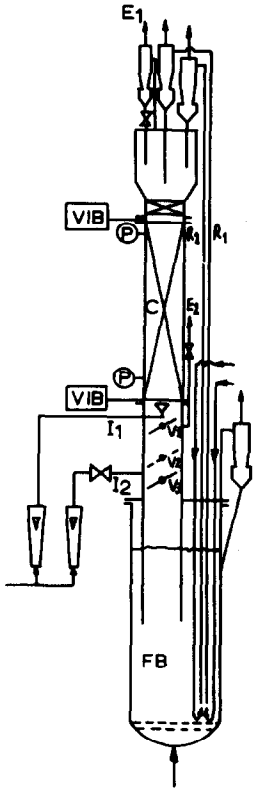

Fig. 2. Experimental set-up; C, column; I, 1,2 gas inlet; E, 1,2 gas outlet; FB, fluid bed; R_1, R_2, risers; V_1, V_2, V_3, valves; VIB, vibrator.

a disengaging section and leaves the column via a cyclone where the entrained solid is removed from the air stream. Two venturies are inserted in the fluid bed and connected with the risers R_1 and R_2 ending in two cyclones. With the help of these pneumatic transport lines particles are fed to the column. As is practised in gas–liquid columns, for the sake of initial distribution of the solids over the column a layer of about 5 cm PALL rings is inserted in the disengaging section of the column.

The gas flow is measured with a rotameter; the solid flow rate is measured integrally. After closing V_2, particles are collected on top of this valve and after a short time V_1 and V_3 are also closed. Now a fluid bed is created in the column which can be fluidized with air coming through I_2 and leaving via E_2. After fluidizing for a few seconds the air flow is interrupted suddenly and the bed slowly settles in a reproduceable way to a fixed bed. From the internal diameter of the section (0.070 m) the fixed bed density and the collection time, the mass flow can be

TABLE 1

Properties of the column packing

	L_{ring} (m)	D_{ring} (m)	δ (m)	a ($m^2\ m^{-3}$)	ϵ_p	N (m^{-3})
PALL rings	0.015	0.015	0.002	310	0.86	2.2×10^5
RASCHIG rings	0.010	0.010	0.001	440	0.80	7.0×10^5
Cylindrical screens	0.010	0.010	0.0005	507	0.97	6.1×10^5

TABLE 2

Properties of the solid particles

Composition: 87 wt.% SiO_2, 12 wt.% Al_2O_3

Particle diameter distribution (sieve analysis):

Diameter (μm)	*Wt. %*	*Cum. wt. %*
<44	7.3	7.3
44 - 75	30.5	37.8
75 - 105	23.9	61.7
105 - 150	36.9	98.0
150 - 210	1.6	99.6
210 - 300	0.3	99.9
>300	0.1	100.0

Mean particle diameter:	$\pm 70 \times 10^{-6}$ m
Skeletal density:	2200 kg m^{-3}
Particle density:	813 kg m^{-3}
Fixed bed density[a]*:*	475 kg m^{-3}
Particle void fraction:	0.63
Fixed bed void fraction[a]*:*	0.78
Terminal velocity of mean particle:	0.15 m s^{-1}

[a]Settled bed after fluidization.

calculated. In this way a mass flow measurement is converted into a simple accurate volumetric determination. Solid flow can be adjusted by changing the airflow through the risers.

Three types of packing have been used; their properties are listed in Table 1. It was possible to operate the column with all packings. PALL rings, however, were clearly superior because of operation flexibility, static hold-up and solid spreading [10]. For these reasons this article mainly presents results for PALL rings. Although some results for the other types are given, these results will be published elsewhere [10]. The solid was a silica–alumina catalyst (a class-A powder according to Geldart [11]); its properties are shown in Table 2.

Pressure drop is measured with a micromanometer at pressure taps along the column wall. As in gas–liquid systems [12], hold-up in gas–solid systems can be split up into two parts, namely the dynamic hold-up (or operating hold-up) and the static hold-up. The first of these can be measured by simultaneously shutting off the air stream to risers R_1 and R_2 and closing valve V_2 to collect the solid which is draining off the packing. The weight of the solid can be measured in the way described above. As the apparent particle density is known, the hold-up can be calculated. The static hold-up can be measured in the same way after vibrating the column with two vibrators (VIB) for one minute at zero gas flow rate. Nearly all static hold-up drains from the packing. The permanent fraction of the static hold-up which remained on the packing after vibration was measured separately by dismounting the column once and weighing the solid matter.

The loading point can be established from dynamic hold-up measurements; it is reached as the dynamic hold-up starts to increase with increasing gas flow rate at constant solid flow.

The flooding point is reached if the dense phase inversion (bubble formation) occurs simultaneously with a sharp increment of pressure drop and hold-up.

2. RESULTS

2.1. Pressure drop

In Fig. 3 the pressure drop per unit column length for PALL rings is plotted *versus* the superficial gas velocity for different solid flow rates. In gas–liquid systems the curves have the same shape [13].

For one solid flow rate, the pressure drop is increasing owing to an increase in the gas velocity itself and the fraction of the solid which is suspended. Since pressure drop is mainly caused by suspended solid and since this suspended fraction is slowly increasing with increasing gas velocity (Fig. 4) at low gas rates the slope is smaller than unity. Beyond the loading point the increasing solid inventory in the column gives an extra contribution.

If the line F–F′ is reached, hold-up and pressure drop rise sharply. An unstable region is reached called flooding.

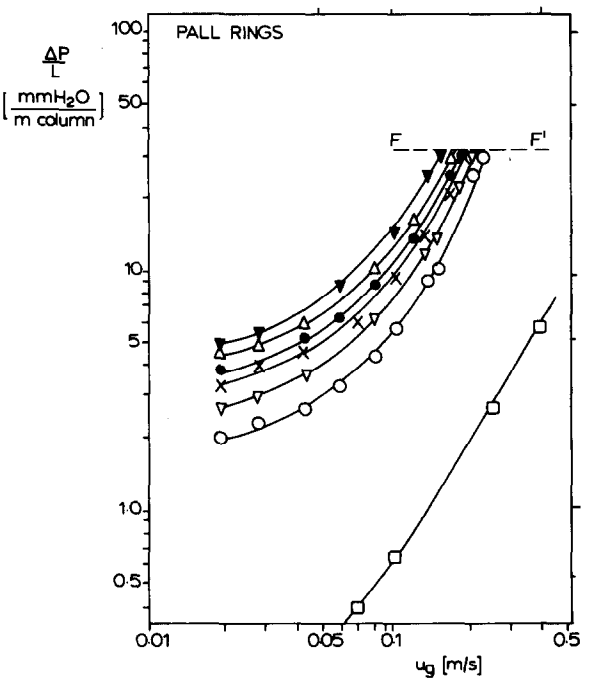

Fig. 3. Pressure drop *vs.* superficial gas velocity.

Symbol:	□	○	▽	×	●	△	▼
S:	0	1.32	2.08	2.91	3.59	4.66	6.13

In Fig. 4 we have plotted

$$\gamma = \frac{\text{(pressure drop with dynamic hold-up)} - \text{(pressure drop without dynamic hold-up)}}{\text{pressure drop in case of full suspension of dynamic hold-up}}$$

or

$$\gamma = \frac{(\Delta p/L)_{\text{incl}\,\beta_{\text{dyn}}} - (\Delta p/L)_{\text{excl}\,\beta_{\text{dyn}}}}{(\rho_P - \rho_g) g \beta_{\text{dyn}}} \qquad (1)$$

γ can be considered to be the fraction of the dynamic hold-up that is freely suspended in the gas phase. Catalyst supported by the packing contributed much less to the pressure drop than suspended catalyst. For example, a packing containing only the static hold-up (β_{st} = 0.023) had a pressure drop only 1% higher than a clean packing. The maximum total hold-up β_{tot} in the experiments was 0.098. For these conditions the pressure drop increases by a factor of 25 over that of the empty packing, which will be mainly due to suspended catalyst.

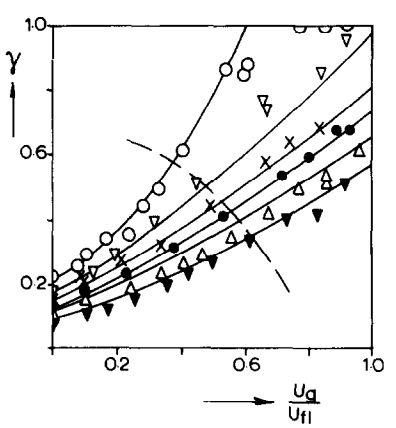

Fig. 4. Fraction of dynamic hold-up which is suspended *vs.* dimensionless gas velocity. For the symbols see Fig. 3. ——, calculated according to eqn. (2); – – –, loading point calculated according to eqn. (5).

The points in Fig. 4 are calculated according to eqn. (1), the lines being calculated according to correlation (2) which provides an excellent fit:

$$\gamma = S^{-0.5}\{1.15(u_g/u_{fl})^{1.2} + 0.25\} \qquad (2)$$

This relation indicates that relatively more particles are suspended if the gas velocity is increasing and the solid flow is decreasing. The absolute magnitude of the exponents cannot be explained yet.

2.2. Hold-up

The hold-up can be split up into the dynamic or operating hold-up and the static hold-up. Figure 5 shows the dynamic hold-up as a function of the gas velocity at different solid flow rates.

Again in analogy to gas–liquid systems [1], dynamic hold-up, at constant solid flow rate, remains unchanged until the loading point is reached; beyond the loading point the solid inventory of the column increases. Solid hold-up also increases with increasing solid velocity. In Fig. 6 the dynamic hold-up, below the loading point, is plotted *versus* the solid flow rate.

As in gas–liquid systems β_{dyn} is assumed to be proportional to S^n since our results lay on

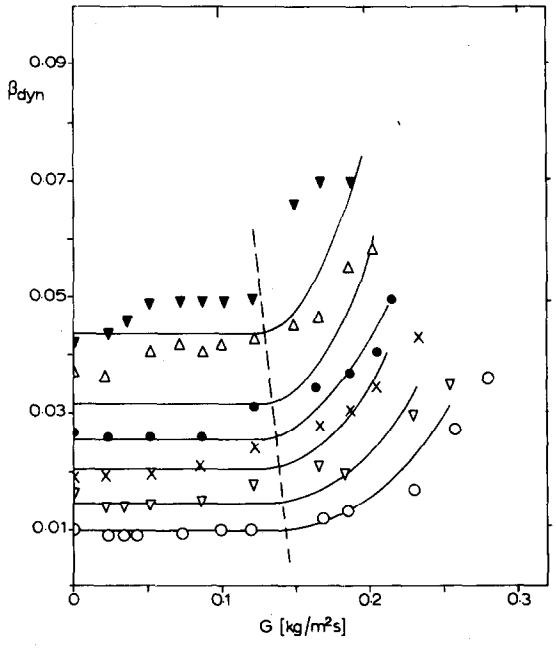

Fig. 5. Dynamic hold-up *vs.* mass flux of gas. For the symbols see Fig. 3. ——, calculated according to eqns. (3) and (4); – – –, loading point calculated according to eqn. (5).

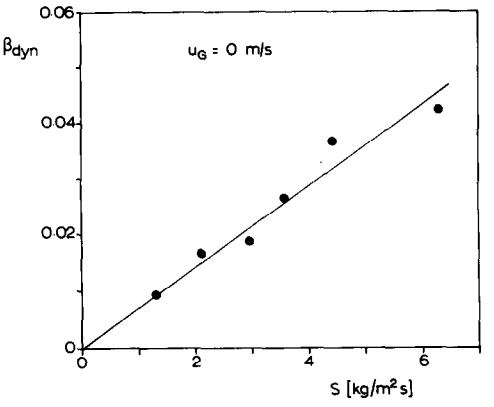

Fig. 6. Dynamic hold-up *vs.* mass flux of solid at zero gas flow rate.

a straight line $n = 1$. This means a constant solid velocity. Claus *et al.* [7, 8] also observed a linear relationship between dynamic hold-up and solid mass flux at zero gas flow rate. In gas–liquid systems an exponent $n = 1/3$ may be expected if a laminar film of liquid flows over the packing. An exponent $n = 1$ means a constant trickle velocity [14, 15]. For wettable packing, an exponent of 0.6 - 0.75 is generally found [16]. For non-wettable packing, *e.g.* if mercury is used as a liquid phase, an exponent of about 0.95 is observed [17, 18].

The constant trickle velocity in the present case is 0.17 m s^{-1} (the terminal velocity of a particle of average diameter is 0.15 m s^{-1}). Claus *et al.* [7, 8], who used sand with particles of mean diameter 235 μm (u_t = 1.79 m s^{-1}), found a trickle velocity of 0.16 m s^{-1}.

With counter-current gas flow the situation becomes different: the gas flow starts to affect the particle behaviour as seen in Fig. 7, which shows a plot of the particle velocity and the slip velocity between gas and particles. At low velocities particle velocity is indeed constant (0.17 m s^{-1}) while at high gas velocities ($u_g/u_{fl} > 0.6$), where γ is increasing, the slip velocity between gas and particles reaches a constant value (0.31 m s^{-1}).

If these velocities are known, the dynamic hold-up can be calculated over the whole range of conditions. Below the loading point the dynamic hold-up can be calculated from

$$u_p = \frac{S}{\beta_{dyn}\rho_p} = 0.17 \text{ m s}^{-1} \qquad (3)$$

From Fig. 5 it can be seen that the dimension-

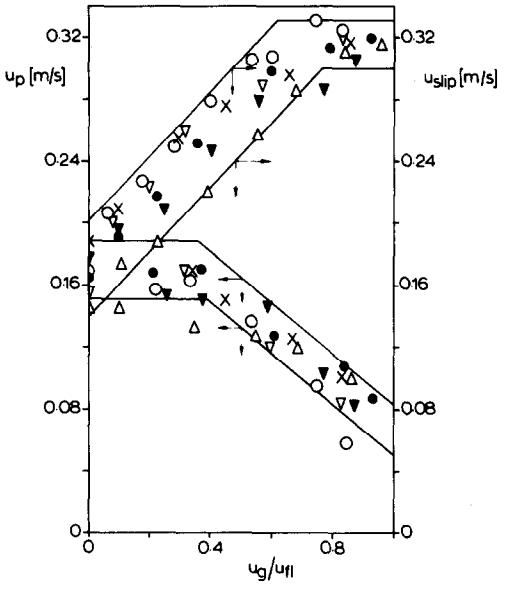

Fig. 7. Particle velocity and slip velocity between gas and particles *vs.* dimensionless gas velocity. For symbols see Fig. 3.

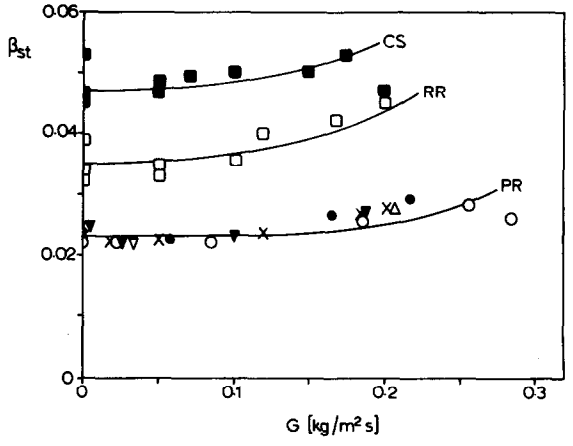

Fig. 8. Static hold-up *vs.* volumetric flux of gas for different packings: ■, cylindrical screens; □, RASCHIG rings. The other symbols represent PALL rings under the same conditions as in Fig. 3.

less gas velocity at the loading point $u_{loading}/u_{fl}$ is about 0.5 - 0.6. Thus beyond the loading point the dynamic hold-up can be estimated from

$$u_{slip} = \frac{S}{\beta_{dyn}\rho_P} + \frac{G}{(\epsilon_p - \beta_{dyn} - \beta_{st})\rho_g} = 0.31 \text{ m s}^{-1} \quad (4)$$

Equations (3) and (4) give the dynamic hold-up over the complete gas velocity range; the lines in Fig. 5 have been calculated in this way.

In Fig. 8 the static hold-up is plotted against the superficial gas velocity at various solid flow rates. The static hold-up is constant at low and slightly increases at high gas velocities. Again this is in line with gas–liquid systems [1]. In gas–liquid systems capillary forces determine the static hold-up [19] while in gas–solid systems geometric factors, repose angle and internal fraction angle, are important.

2.3. Loading point

The loading point is reached when the solid inventory increases with increasing gas velocity. Below the loading point the hold-up can be calculated according to eqn. (3) and above the loading point with eqn. (4). At the loading point these two quantities should be equal. Substitution of eqn. (3) into eqn. (4) gives

$$u_{loading} = \frac{G_{loading}}{\rho_g} = \left(\epsilon - \frac{S}{\rho_P u_p}\right)(u_{slip} - u_p) \quad (5)$$

where

$$\epsilon - \frac{S}{\rho_P u_p} = \epsilon_p - \beta_{st} - \beta_{dyn,\,preloading} \quad (6)$$

In eqn. (5) the first term is the void fraction, the second a linear gas velocity. The loading points indicated in Figs. 4 and 5 are calculated from eqn. (5). For gas–liquid systems the gas velocity at the loading point is also decreasing if solid flow is increased [1].

2.4. Flooding point

In gas–liquid systems there are quite a number of definitions of the flooding point [20]. We define the flooding point as the point where the dynamic hold-up, or pressure drop, suddenly rises sharply with increasing gas rate. At the same moment, phase inversion starts (bubbles are formed). A mathematical formulation of this criterion is

$$\left\{\left(\frac{\partial\beta}{\partial u_g}\right)_{flooding}\right\}^{-1} = 0 \quad (7)$$

Inserting eqns. (4) into (7) gives the following expression (8) for the gas velocity at flooding.

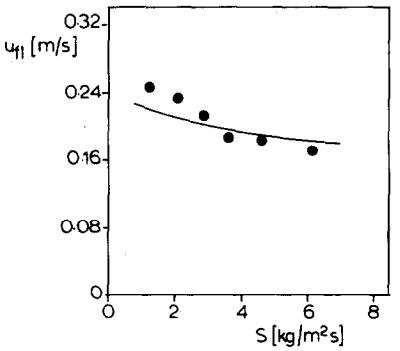

Fig. 9. Gas velocity at flooding *vs.* mass flux of solid: ——, calculated according to eqn. (8); •, experimental.

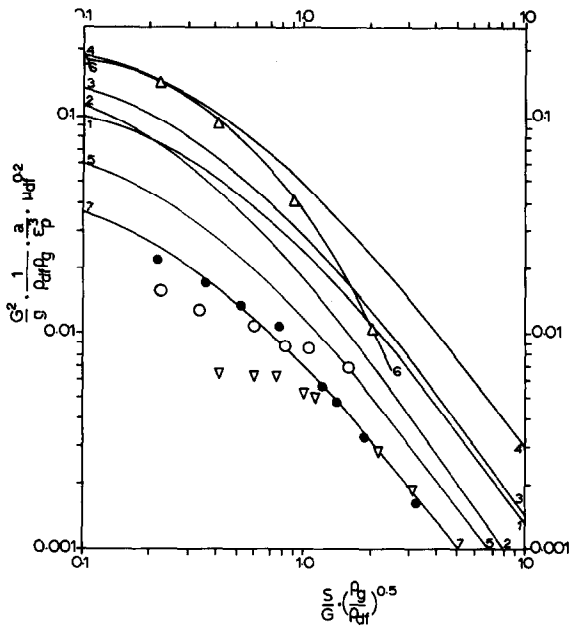

Fig. 10. Flooding correlations: 1, Sherwood *et al.*; 2, Lobo *et al.*; 3, Zenz; 4, Standish, non-wetting flow; 5, Standish, wetting with foam; 6, Claus *et al.*, air-sand, symbol △; 7, present investigation.

Symbol	Packing
•	RASCHIG rings
○	PALL rings
▽	Cylindrical screens

$$u_{fl} = \frac{G_{fl}}{\rho_g} = \left\{ \epsilon^{1/2} - \left(\frac{S}{\rho_p u_{slip}} \right)^{1/2} \right\}^2 u_{slip} \qquad (8)$$

From this equation, it is clear that the flooding gas velocity is decreasing as expected if the solid velocity is increasing. The experimental data and equation (8) are presented in Fig. 9.

A fluidized bed is sometimes considered to behave as a viscous liquid [21]. Similarly, solid flow is assumed to behave as liquid flow. The properties of the simulated liquid are equal to the fluid bed properties under dense phase conditions [22]. In this way the measured flooding points can be related to flooding plots for gas–liquid systems. The results of the latter are usually correlated in modifications of the Sherwood plot [23 - 26]. Figure 10 shows our results for the air catalyst system using various packings. The results obtained by Claus *et al.* [7, 8] and those for gas–liquid systems are also given. The viscosity of our catalyst was assumed to be 5×10^{-3} N s m^{-2}, a value measured by Matheson for a comparable cracking catalyst, using a paddle viscosity meter [27]. The value for the sand used by Claus *et al.* [7, 8] was taken as 0.5 N s m^{-2}, measured for quartz sand by Schügerl [28]. Fortunately the ordinate is not very sensitive to variations in viscosity. From Fig. 10 it can be seen that the general shape of the curves is more or less the same; nevertheless the data for gas–liquid packed columns cannot be used for our system. Equation (8) can also be written in another form:

$$\left(\frac{G}{\rho_g}\right)^{1/2} + \left(\frac{S}{\rho_p}\right)^{1/2} = (\epsilon u_{slip})^{1/2} \qquad (9)$$

Wallis [29] and Dill and Pratt [30] found a similar relation for gas–liquid systems.

$$\left(\frac{G}{\rho_g}\right)^{1/2} + \left(\frac{\rho_f}{\rho_g}\right)^{1/4}\left(\frac{L}{\rho_f}\right)^{1/2} = 0.78\left(g\,\frac{\rho_f - \rho_g}{\rho_g}\,\frac{\epsilon_p^3}{a}\right)^{1/4} \qquad (10)$$

Equations (9) and (10) are plotted in Fig. 11.

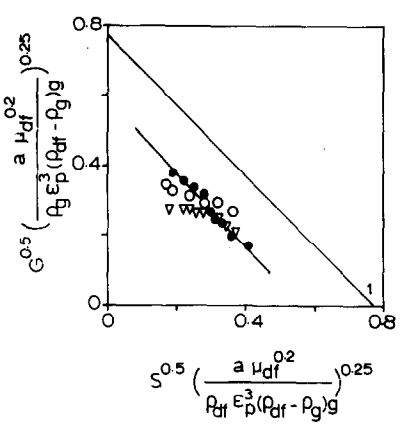

Fig. 11. Wallis plot for flooding: 1, Wallis; 2, present investigation. For symbols see Fig. 10.

The Wallis equation is very useful because it gives a direct mathematical expression that is easy to use in computer calculations; in addition, the ordinate is an independent variable.

3. CONCLUSIONS

Gas–solid packed columns at trickle flow exhibit a behaviour comparable with gas–liquid packed columns. The gas–liquid data, however, cannot be used to predict pressure drop, hold-up, loading or flooding.

For the air-cracking catalyst system with PALL rings as packing material a correlation has been established for the fraction of the dynamic hold-up that is suspended in the air stream. The pressure drop, which is mainly caused by these suspended particles, is very low owing to the fact that the packing carries up to 50% of the solid

At low gas velocities the particle falling rate is constant; however at high gas velocities the slip velocity between gas and solids becomes constant. As these velocities are known, equations can be derived for dynamic hold-up, loading point and flooding point.

ACKNOWLEDGMENT

The authors are indebted to the Dutch State Mines for financial support during the present investigation.

NOMENCLATURE

a	packing surface area per cubic metre of column, $m^2\ m^{-3}$
D_{ring}	ring diameter, m
g	acceleration due to gravity, $m\ s^{-2}$
G	superficial mass flux of gas, $kg\ m^{-2}\ s^{-1}$
L	column length, m
L_f	mass flux of fluid, $kg\ m^{-2}\ s^{-1}$
L_{ring}	height of a ring, m
n	exponent in dynamic hold-up relation
N	number of rings per cubic meter of column, m^{-3}
ΔP	pressure drop, mmH_2O
S	superficial mass flux of solid, $kg\ m^{-2}\ s^{-1}$
u_{fl}	superficial gas velocity at flooding, $m\ s^{-1}$
u_g	superficial gas velocity, $m\ s^{-1}$
$u_{loading}$	superficial gas velocity at loading point, $m\ s^{-1}$
u_p	linear particle velocity, $m\ s^{-1}$
u_{slip}	linear slip velocity between particles and gas, $m\ s^{-1}$
u_t	terminal velocity of mean particle, $m\ s^{-1}$
β_{dyn}	dynamic or operating hold-up
β_{st}	static hold-up
β_{tot}	total hold-up
γ	fraction of dynamic hold-up carried by gas
δ	wall thickness ring
ϵ	$= \epsilon_p - \beta_{tot}$, void fraction
ϵ_p	void fraction of packing
μ_{df}	dynamic viscosity of the gas–solid mixture under dense phase conditions, $N\ s\ m^{-2}$
ρ_{df}	density of the gas–solid mixture under dense phase conditions, $kg\ m^{-3}$
ρ_g	density of gas, $kg\ m^{-3}$
ρ_p	density of particle, $kg\ m^{-3}$
ρ_s	skeletal density of solid, $kg\ m^{-3}$
ρ_f	liquid density, $kg\ m^{-3}$

REFERENCES

1 R. H. Perry and C. H. Chilton, *Chemical Engineers' Handbook*, McGraw-Hill, New York, 1973.
2 C. Berg, *Chem. Eng. Prog.*, *47* (1951) 585.
3 R. Ullrich, *Chem. Technol.*, *26* (1974) 278.
4 Y. B. G. Varma, *Powder Technol.*, *12* (1973) 167.
5 S. Morooka, M. Nishinaka and Y. Kato, *Int. Chem. Eng.*, *17* (1977) 254.
6 I. O. Protodyakonov, P. G. Romankov and A. G. Samsonov, *J. Appl. Chem. USSR (Eng. Transl.)*, *45* (1972) 1185.
7 G. Claus, F. Vergnes and P. Le Goff, *Fluid. Techn. Proc. Int. Fluid Conf., Asilomar, 1975*, Hemisphere, Washington, 1976.
8 G. Claus, F. Vergnes and P. Le Goff, *Can. J. Chem. Eng.*, *54* (1977) 143.
9 A. W. M. Roes and W. P. M. van Swaaij, to be published.
10 A. W. M. Roes, *Thesis*, Twente University of Technology.
11 G. Geldart, *Powder Technol.*, *7* (1973) 285.
12 M. R. Fenske, C. O. Tongberg and D. Quiggle, *Ind. Eng. Chem.*, *26* (1934) 1169.
13 J. S. Eckert, *Chem. Eng.*, *82* (1974) 493.

14 B. E. Hutton, L. S. Leung, P. C. Brooks and D. J. Nicklin, *Chem. Eng. Sci., 29* (1974) 493.
15 J. E. Buchanan, *Ind. Eng. Chem. Fundam., 6* (1967) 400.
16 D. M. Mohunta and G. S. Laddha, *Chem. Eng. Sci., 20* (1965) 1069.
17 N. A. Warner, *Chem. Eng. Sci., 11* (1959) 149.
18 N. Standish, *Chem. Eng. Sci., 23* (1968) 51.
19 W. P. M. van Swaaij, J. C. Charpentier and J. Villermaux, *Chem. Eng. Sci., 24* (1969) 1083.
20 F. C. Silvey and G. J. Kelly, *Chem. Eng. Prog., 62* (1966) 68.
21 J. F. Davidson and D. Harrison, *Fluidised Particles*, Cambridge University Press, London, 1963.
22 W. P. M. van Swaaij and F. J. Zuiderweg, *Proc. Int. Symp. Fluid. Appl., Toulouse, 1973*, Cepadues, Toulouse, p. 454.
23 T. K. Sherwood, G. H. Shipley and F. A. L. Halloway, *Ind. Eng. Chem., 30* (1938) 965.
24 W. E. Lobo, L. Friend and F. A. Zenz, *Am. Inst. Chem. Eng., 41* (1943) 109.
25 F. A. Zenz, *Chem. Eng. Prog., 43* (1947) 415.
26 N. Standish and J. B. Drinkwater, *J. Met., 24* (1972) 43.
27 G. L. Matheson, W. A. Herbst and P. H. Holt, *Ind. Eng. Chem., 41* (1949) 1099.
28 K. Schügerl, in J. F. Davidson and D. Harrison (eds.), *Fluidisation*, Academic Press, London, 1971.
29 G. B. Wallis, *One Dimensional Two Phase Flow*, McGraw-Hill, New York, 1969.
30 F. R. Dell and H. R. C. Pratt, *Trans. Inst. Chem. Eng., 29* (1951) 89.